Design and Analysis of Completely Adiabatic Tapered Waveguides by Conformal Mapping

Ching-Ting Lee, *Member, IEEE,* Mount-Learn Wu, Lih-Gen Sheu, Ping-Lin Fan, and Jui-Ming Hsu

***Abstract*— In this study, we propose a novel equivalent-waveguide concept to design the completely adiabatic tapered waveguides. The optimal combination of taper shape and refractive-index distribution in such ideal structures is obtained by applying a series of conformal mappings to transform a single-mode straight waveguide into an equivalent tapered configuration. In an ideal taper the curved phase-front effect verifies the constant V-number concept is insufficient for designing a tapered waveguide. Also, the beam propagation method combined with the conformal mapping method is used to analyze the characteristics of light propagation in ideal structures. Simulation results predict that in the ideal taper a perfect mode-size conversion can be achieved adiabatically.**

I. Introduction

IN INTEGRATED optics, tapered waveguides offer an excellent means of converting optical mode sizes [1]–[4] to connect optical devices of different cross-sectional dimensions. To achieve a highly efficient power-coupling, the guided mode should propagate through the tapered waveguide adiabatically. This fact implies that the structure must operate under radiation-loss-free and mode-conversion-free conditions [5]–[7]. Therefore, it is desirable to maintain the first-order mode in the waveguide without mode conversion to higher order modes or to radiation modes taking place.

A number of methods [4], [8]–[13] for increasing the coupling efficiency of tapered waveguides are already available in the literature. These approaches can be classified into three categories: cross-sectional dimension tapering [8]–[10], index tapering [11], or a combination of both [4], [12], [13]. To demonstrate the completely adiabatic concept, the normalized frequency V of tapered waveguides is investigated. It has been proposed in several papers [1], [4]–[6] that the normalized frequency V of a waveguide must be kept constant to maintain single-mode operation throughout the tapered structure. According to normalized-frequency definition, the V number of dimensional tapered waveguides varies with the nonuniform cross-section. For this reason, such waveguides cannot operate in completely adiabatic conditions. Although the V-number concept cannot be directly applied to a waveguide with index-tapering in the propagation direction [5], the concept of local normal modes makes such kind of structures easy to describe by the V number. Similarly, the V number in an index-tapering waveguide structure is not constant. Consequently, the completely adiabatic tapered waveguides can be achieved only by simultaneously altering the refractive index and the cross-section of structures.

However, in designing the tapered waveguides of variable width and index, the problem of optimizing the taper shape and the refractive-index distribution in such structures arises. It is a well-known fact that a single-mode straight waveguide with homogeneous refractive-index distribution along the propagation direction has the adiabatic property (i.e., its V number is constant). Therefore, it is desirable that a completely adiabatic tapered waveguide behaves similar to the straight structure and possesses the capacity to convert optical mode sizes.

Section II describes using the conformal mapping method how the single-mode straight waveguide is transformed into an equivalent tapered structure. The transformation results in an optimal combination of taper shape and refractive-index distribution in a completely adiabatic tapered waveguide. The relationship between refractive-index variation and taper length (or taper shape) is discussed in detail. In addition, by applying the conformal mapping method the phase front of guide mode propagating in the taper is constructed. The curved phase front in the taper reveals important mode-field properties; however, all of the proposed structures neglect this phenomenon. The influence of curved phase front on the design and analysis of tapered waveguides is a relevant topic in this paper. Finally, the transmission characteristics of the completely adiabatic tapered waveguide are analyzed by using the beam propagation method combined with the conformal mapping method. The analysis verifies that the predicted mode-size conversion and the completely adiabatic performance in the ideal structures are accomplished.

II. Analysis Method

Fig. 1(a) presents a slab dielectric waveguide structure with an abrupt transition. This waveguide is uniform along the y direction. Assuming the fundamental TE mode in the waveguide, the modal field is solved by the scalar Helmholtz equation

$$(\nabla_{z,x}^2 + n^2(z,x)k_0^2)E = 0 \tag{1}$$

where E is the electric field amplitude, $k_0 = 2\pi/\lambda$ is the free-space wavenumber, $n(z,x)$ is the refractive index as a function of position, and $\nabla_{z,x}^2$ is the two-dimensional (2-D) Laplacian in a coordinate system z,x. Basically, the abrupt waveguide transition is the simplest version used to connect waveguides

Manuscript received June 17, 1996; revised October 22, 1996. This work was supported by the National Science Council of the Republic of China under Contract NSC83-0417-E-008-004.

The authors are with the Institute of Optical Sciences, National Central University, Chung-Li, Taiwan, Republic of China.

Publisher Item Identifier S 0733-8724(97)01358-3.

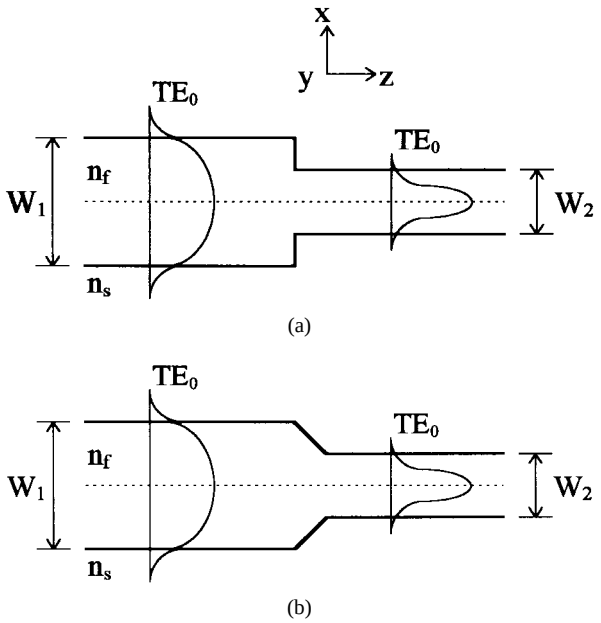

Fig. 1. Schematic illustration of waveguide transition: (a) abrupt transition and (b) tapering transition.

of different cross-sectional dimensions. Power transfer at such an abrupt discontinuity was readily calculated in several papers [14]–[16]. Those works demonstrated that the ratio in the widths of input and output ends W_1/W_2 should be restricted to an extremely small range in order to avoid excessive radiation losses. Therefore, the tapered waveguide shown in Fig. 1(b) is the means commonly used to convert the optical mode size.

In this work, the waveguide structure with an abrupt transition is selected as a prototype to propose an ideal structure of the completely adiabatic tapered waveguide. Fig. 2(a) is a schematic diagram illustrating the abrupt transition waveguide along with an undefined area (used to connect two straight regions) in the discontinuity section. Owing to modal field penetration, the abrupt transition structure should be completely contained in a larger analyzed domain to take the whole optical power into consideration. Since this waveguide structure is intended for completely adiabatic performances, the conversion of optical mode sizes should be achieved in the output end. Thus, a smaller analyzed domain is assumed in the output end than that in the input end. The widths at the input and output ends of the analyzed domain are denoted as W_{A1} and W_{A2}, respectively. The ratio of W_{A1} to W_{A2} is defined as

$$\frac{W_{A1}}{W_{A2}} = \frac{W_1}{W_2} \tag{2}$$

where W_1 and W_2 are the widths at the input and output ends of the waveguide structure. Consequently, the analyzed domain maintains the same shape as the abrupt transition waveguide.

To determine both the shape and the refractive-index distribution in the completely adiabatic tapered waveguide, the single-mode straight waveguide in a strip-shaped domain of φ plane [Fig. 2(b)] is adopted as an equivalent structure. The width of the strip-shaped domain is denoted as W_{A1}, which is equal to the width at the input end of the analyzed domain

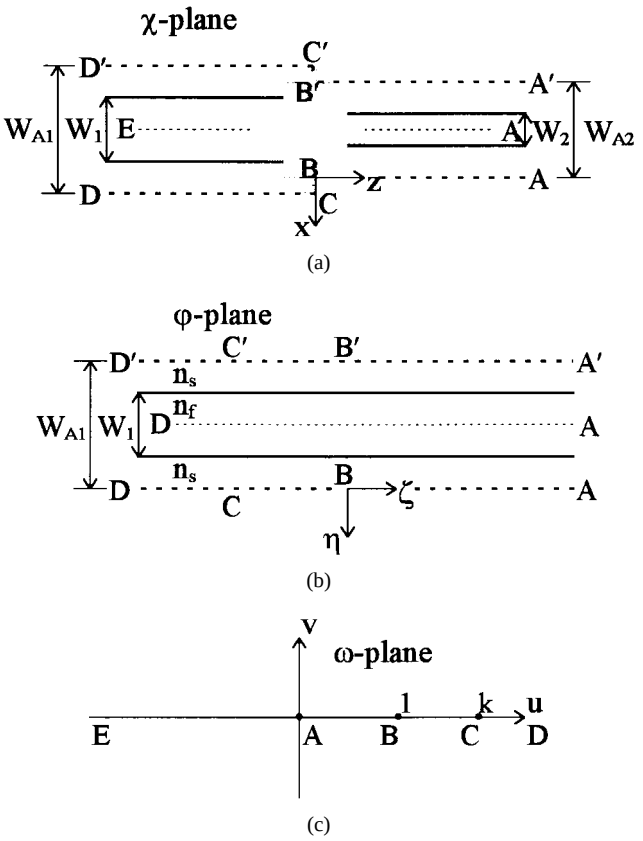

Fig. 2. Conformal mappings for the completely adiabatic structures. (a) The abrupt transition waveguide with an undefined area in the discontinuity section (the final transformed geometry in the χ plane). (b) The single-mode straight waveguide (the original configuration in the φ plane). (c) The intermediate transformed domain $(v \geq 0)$ in the ω plane.

shown in Fig. 2(a). The purpose of conformal mapping is to transform the strip-shaped domain of φ plane into the analyzed domain of χ plane. The shapes of these two analyzed domains should possess the geometrical characteristics of waveguides located in them. Because the strip-shaped domain is symmetric with respect to the center line (the dashed line in the straight waveguide), the following transformations are available for both the upper and lower half portions. Here, the lower one is used to demonstrate the transformation process. First, the lower half portion in the strip-shaped domain is mapped into the upper half ω plane of Fig. 2(c) by

$$\omega = \exp\left(\frac{-2\pi\varphi}{W_{A1}}\right). \tag{3}$$

Then, using the Schwarz–Christoffel transformation, the upper half ω plane is mapped into the lower half portion of the initial analyzed domain (χ-plane). Its mapping formula is expressed as

$$\chi = \frac{W_{A1}}{2\pi}\int_1^{\omega} \frac{-1}{\omega}\left(\frac{\omega-1}{\omega-k}\right)^{1/2} d\omega \tag{4}$$

where $k>1$ and its exact value will be determined later. The variable change for integrating the above equation is made by

$$m = \left(\frac{\omega-1}{\omega-k}\right)^{1/2}. \tag{5}$$

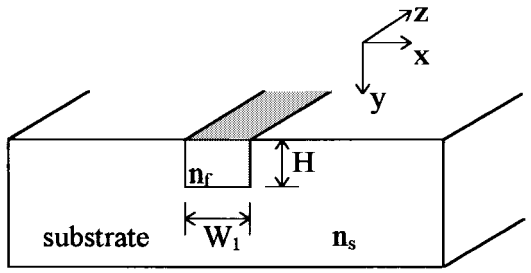

Fig. 3. The geometry of a 3-D embedded waveguide.

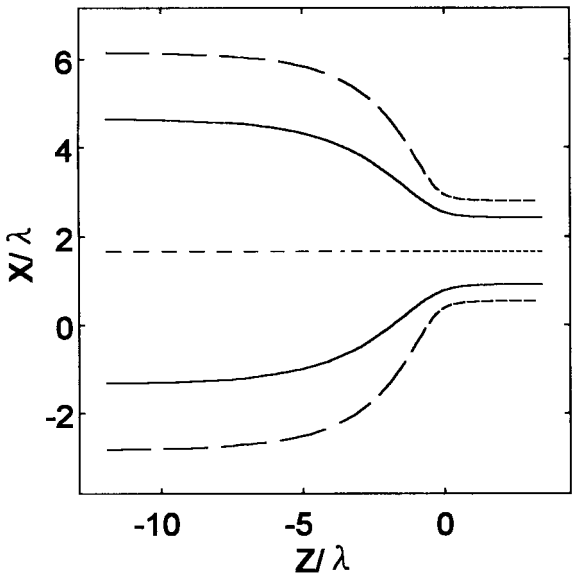

Fig. 4. The waveguide shape (solid lines) for the completely adiabatic tapered structure with $W_1/W_2 = 4$ and $W_{A1} = 20$ μm. The dashed lines inside and outside the waveguide represent the center line and the effective waveguide width, respectively.

After some mathematical manipulations, the transformation formula can be expressed as

$$\chi = \frac{-W_{A1}}{2\pi}\left[\ln\frac{1+\left(\dfrac{\omega-1}{\omega-k}\right)^{1/2}}{1-\left(\dfrac{\omega-1}{\omega-k}\right)^{1/2}} - \frac{1}{\sqrt{k}}\ln\frac{1+\sqrt{k}\left(\dfrac{\omega-1}{\omega-k}\right)^{1/2}}{1-\sqrt{k}\left(\dfrac{\omega-1}{\omega-k}\right)^{1/2}}\right]. \quad (6)$$

In the above equation, if $\omega = k$ is substituted, the k value is obtained as

$$k = \left(\frac{W_{A1}}{W_{A2}}\right)^2. \quad (7)$$

Using (3) and (6), the straight waveguide of Fig. 2(b) can be transformed into the equivalent tapered structure [Fig. 2(a)]. Thus, the shape of undefined area in the abrupt discontinuity is derived. This equivalent tapered structure is ideal for the adiabatic tapered waveguide. Its characteristics are thoroughly investigated in Section III.

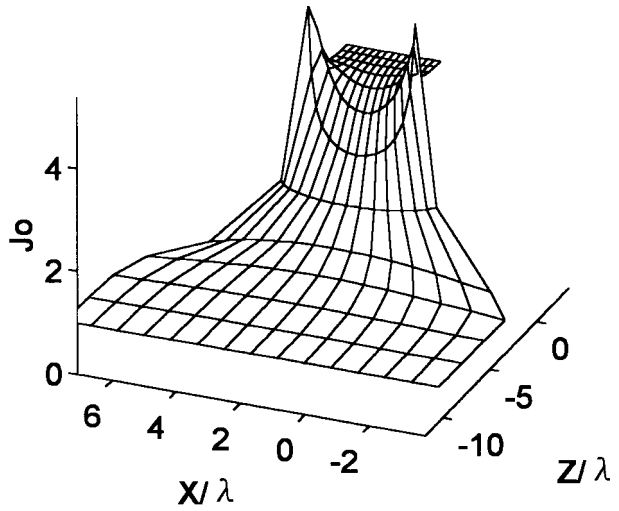

Fig. 5. The Jacobian-determinant variation in the tapered region of the completely adiabatic tapered structure (the case of $W_1/W_2 = 4$ and $W_{A1} = 20$ m).

The remaining problem is to deal with the refractive-index distribution in the ideal structure. If the coordinate transformation in 2-D simulations is a conformal mapping, the coordinate variables satisfy the Cauchy–Riemann relations. By applying these relations to (1), the scalar Helmholtz equation in the equivalent tapered structure (χ-plane) can be restated as

$$\left(\nabla_{z,x}^2 + \left|\frac{d\varphi}{d\chi}\right|^2 \tilde{n}^2(\zeta,\eta)k_0^2\right)E = 0 \quad (8)$$

where $\tilde{n}(\zeta,\eta)$ is the refractive index in the straight waveguide (φ-plane) and $|d\varphi/d\chi|$ is the Jacobian determinant J_0 of the transformation as defined by

$$J_0 = \left|\frac{d\varphi}{d\chi}\right| = \left|\left(\frac{\exp\left(\dfrac{-2\pi\varphi}{W_{A1}}\right)-1}{\exp\left(\dfrac{-2\pi\varphi}{W_{A1}}\right)-k}\right)^{-1/2}\right|. \quad (9)$$

Consequently, the refractive index in the ideal tapered waveguide (χ-plane) is

$$n(z,x) = \left|\left(\frac{\exp\left(\dfrac{-2\pi\varphi}{W_{A1}}\right)-1}{\exp\left(\dfrac{-2\pi\varphi}{W_{A1}}\right)-k}\right)^{-1/2}\right|\tilde{n}(\zeta,\eta). \quad (10)$$

III. Results and Discussion

To demonstrate the ideal tapered waveguide with an optimal combination of cross-sectional dimension and refractive-index distribution, a three-dimensional (3-D) embedded straight waveguide (Fig. 3) is selected as the equivalent structure in conformal transformations. The associated geometrical and dielectric parameters of the straight waveguide are as follows: $W_1 = 9$ μm, $H = 6.9$ μm, $n_s = 1.5$, and $n_f = 1.504$. The wavelength λ of a fundamental TE mode is assumed to be 1.5 μm. With the above values, the effective width W_{eff} of the waveguide is calculated to be 13.5 μm. To take full account

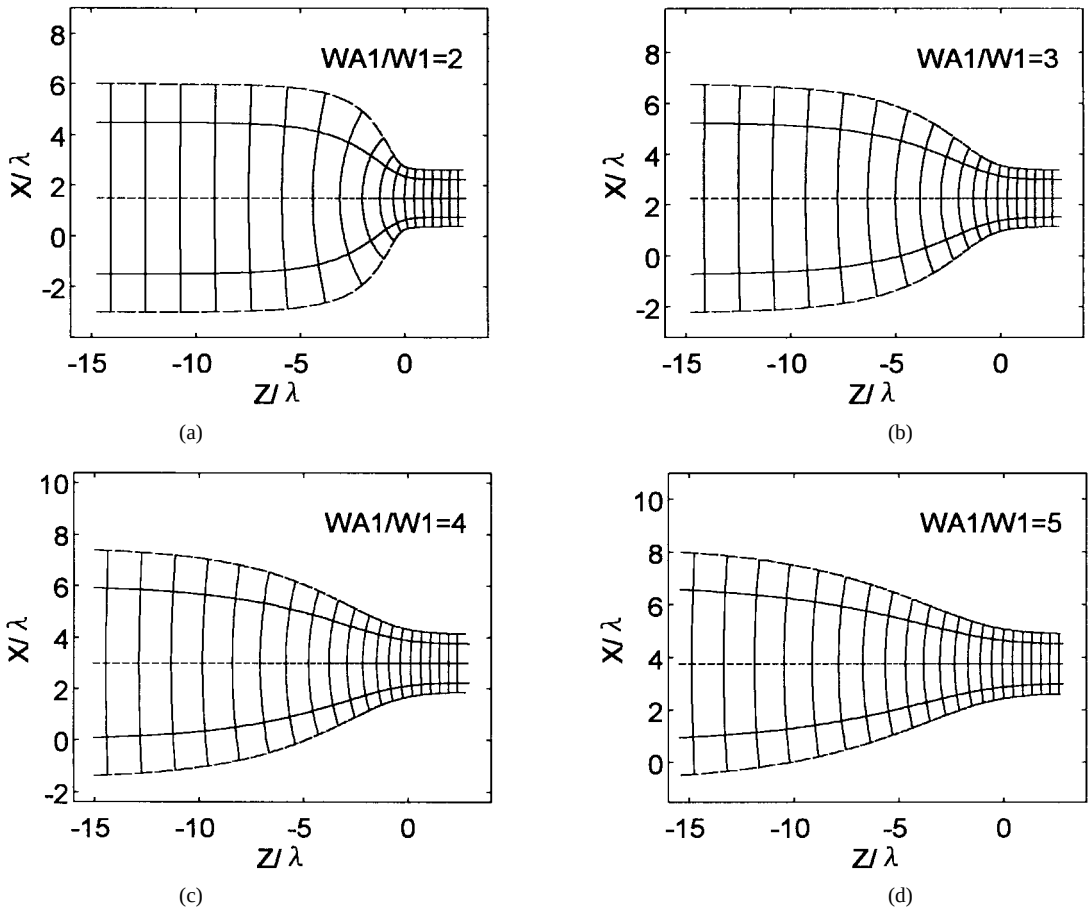

Fig. 6. Schematic diagrams of the mapped phase fronts propagate in the ideal tapered waveguides (the case of $W_1/W_2 = 4$) with (a) $W_{A1}/W_1 = 2$; (b) $W_{A1}/W_1 = 3$; (c) $W_{A1}/W_1 = 4$; (d) $W_{A1}/W_1 = 5$. The dashed lines inside and outside the waveguide represent the center line and the effective waveguide width, respectively.

of the optical power in the waveguide, the width W_{A1} of the analyzed domain is set to be greater than W_{eff}.

A. Ideal Tapered Waveguides

Fig. 4 shows a completely adiabatic tapered waveguide with $W_1/W_2 = 4$ and $W_{A1} = 20$ μm. The dashed lines inside and outside the ideal structure represent the locus of light propagation and the effective waveguide width, respectively. These dashed lines are mapped from the corresponding ones in the equivalent straight waveguide. The waveguide-width variation in the tapered region is continuous along the propagation direction. Fig. 5 illustrates the Jacobian determinant J_0 of the transformation within the effective width of an ideal tapered waveguide (the case of $W_1/W_2 = 4$ and $W_{A1} = 20$ μm). As indicated in this figure, the values of J_0 at the input and output ends of the tapered waveguide are equal to 1 and 4, respectively. While for the tapered region, the values of J_0 vary from 1 to 4 as the waveguide width reduces from W_1 to W_2 (equal to $0.25W_1$). According to (10) in Section II, the Jacobian determinant J_0 gives the same tendency of refractive indexes. Under intuitive observations about variation in index and width, the normalized frequency V seems to remain constant along the propagation direction. This fact ensures that the first-order mode propagates throughout the waveguide without any mode conversion. However, the values of J_0 in the tapered region are not constant along the transverse direction (x-direction). This inhomogeneous distribution is interpreted in Section III-B.

In (3), the mapping formula is a function of W_{A1}. Since the coordinates of ω plane are related to the width W_{A1} of the analyzed domain, W_{A1} is also a variable in (6). Fig. 6(a)–(d) are the schematic diagrams of the ideal configurations together with the phase fronts within the effective widths of tapered waveguides with $W_1/W_2 = 4, W_{A1}/W_1 = 2, 3, 4$, and 5. For small values of W_{A1}, the waveguide-width transition in the tapered region is very sharp. Moreover, the taper length is diminished as W_{A1} reduces. This finding obviously implies that one straight waveguide can be transformed into equivalent tapered structures with different taper lengths by selecting the value of W_{A1}. These equivalent structures would perform the same function. The only difference in these structures is that the speed of optical mode-size conversion is dependent on the taper length. The conversion of mode sizes would vary faster in a shorter taper but more slowly in a longer one. According to the definition of (9), the Jacobian determinant J_0 is also a function of W_{A1}. Fig. 7 describes the variation in Jacobian determinant J_0 on the center line of the tapered waveguide along the propagation direction for various values of W_{A1}/W_1. As indicated in this figure, an

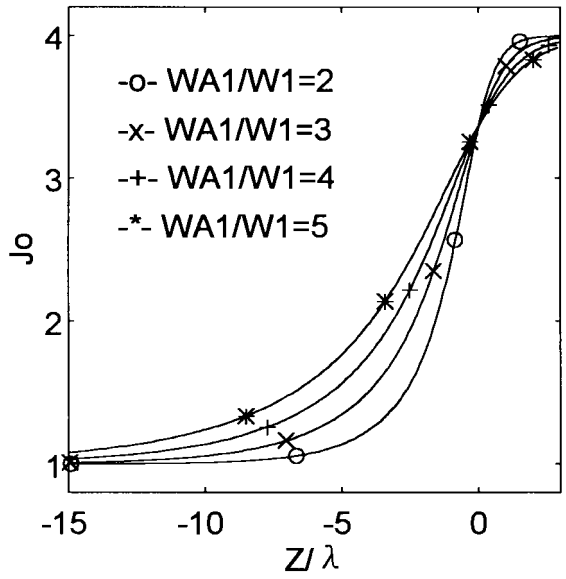

Fig. 7. The Jacobian-determinant variation on the center line of ideal tapered waveguides (the case of $W_1/W_2 = 4$) with different ratios of W_{A1}/W_1.

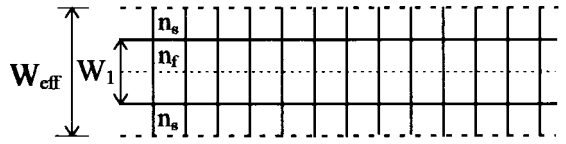

Fig. 8. Schematic view of the phase fronts propagating in a straight waveguide. The dashed lines inside and outside the waveguide represent the center line and the effective waveguide width, respectively.

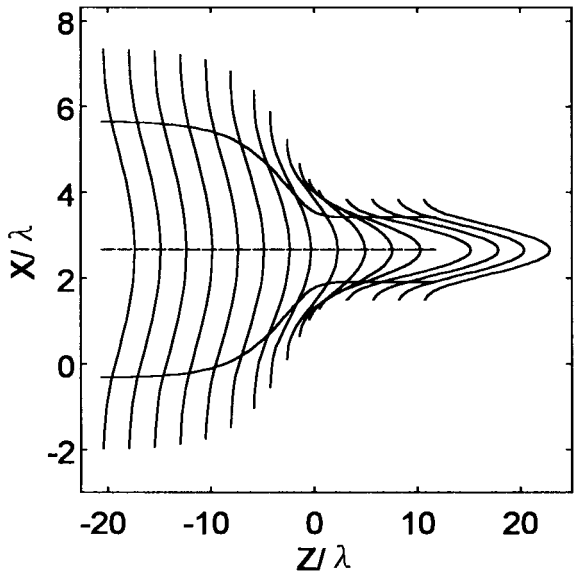

Fig. 9. The power distribution of modal field in the ideal tapered waveguide with $W_1/W_2 = 4$ and $W_{A1} = 32$ μm.

reduction in W_{A1} causes the strong variation in J_0. Therefore, the taper shape and the refractive-index distribution of ideal tapered waveguides can be controlled by selecting the width W_{A1} of an analyzed domain. This fact suggests that a wide-angle tapered waveguide with the adiabatic characteristic is achievable theoretically.

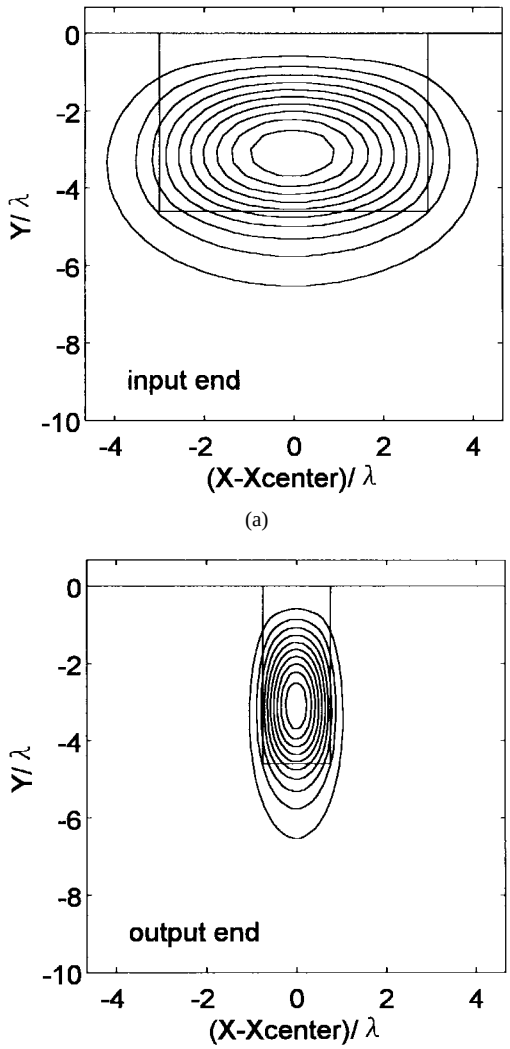

Fig. 10. The field intensity contours of the fundamental TE modes at (a) the input end and (b) the output end of the ideal tapered waveguide with $W_1/W_2 = 4$ and $W_{A1} = 32$ μm. Xcenter represents the lateral position of the center line.

B. Simulation Results of Transmission Characteristics

As can be seen in Fig. 6, the phase front in various ideal structures is the conformal transformation of the planar phase front in an equivalent straight structure (Fig. 8). Notably, the mapped phase front is still normal to the propagation direction throughout the tapered structure. However, the phase front remains a plane in the input and output straight regions but becomes a curved surface in the tapered region.

There are four corners appearing in the tapered waveguide, referred to as outer corners (connecting input straight region and taper) and inner corners (connecting output straight region and taper), respectively. These corners are defined according to the distance between corners and the center line. The evolution of the phase front in an ideal tapered waveguide implies that it should travel faster at the outer corners but slower at the inner corners. This phenomenon is consistent with the distribution of J_0 in the tapered region (Fig. 5), which is relatively small at the outer corners but relatively large at the inner corners. Since the same tendency of refractive-index distribution is obtained

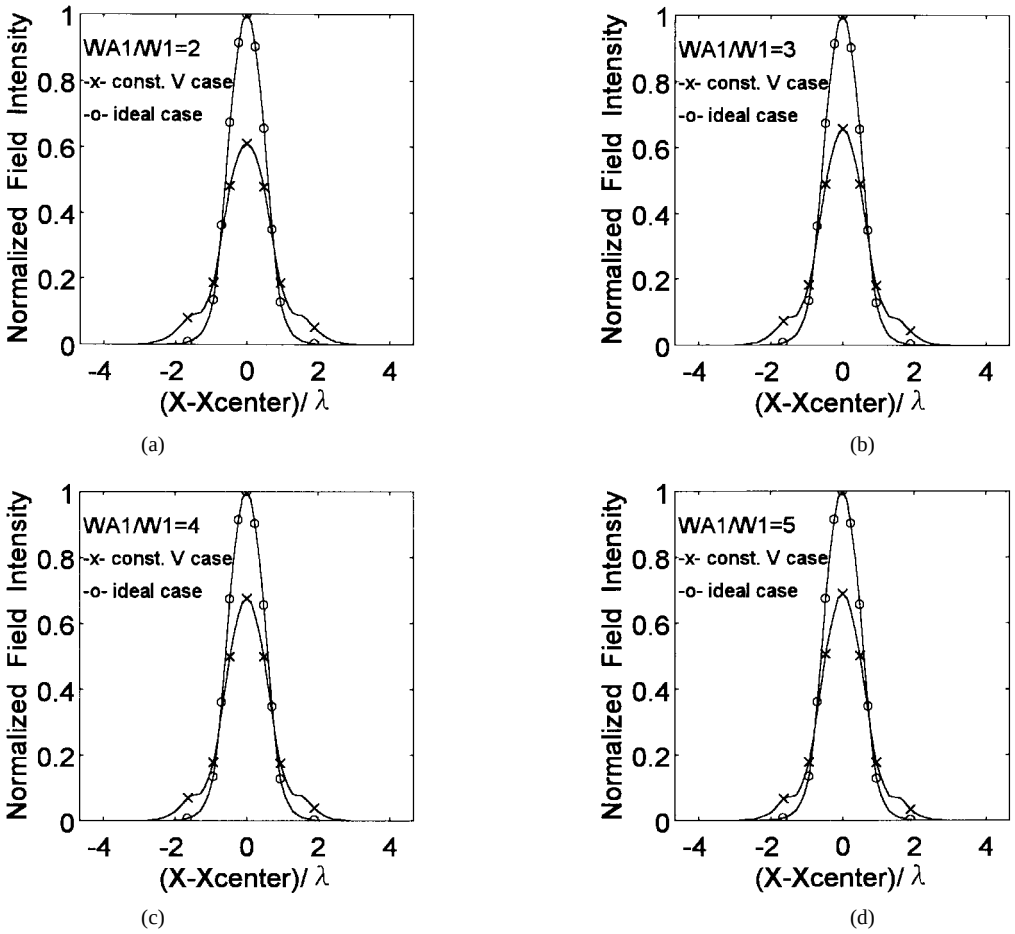

Fig. 11. The normalized field intensity in the constant V-number tapered waveguides with $W_1/W_2 = 4$ and (a) $W_{A1}/W_1 = 2$; (b) $W_{A1}/W_1 = 3$; (c) $W_{A1}/W_1 = 4$; (d) $W_{A1}/W_1 = 5$. Xcenter represents the lateral position of the center line.

in a tapered structure as J_0, such index distribution makes the input and output ends of the taper region behave similar to the convex and concave lenses, respectively. Therefore, the reduction in width of a phase front can be achieved in a completely adiabatic taper.

In a straight waveguide (Fig. 8), the normalized frequency V of every planar phase front is constant. Therefore, in its equivalent tapered structure, the V number of the corresponding curved phase front is still constant. This fact suggests that the V number in a taper is no longer constant along the propagation direction. However, the previously proposed tapers were designed by applying the constant V-number concept. According to the concept of local normal modes, the phase fronts passing through those tapered structures were assumed to be planar. As illustrated in Fig. 6, if the conversion of optical mode sizes occurs in a taper, its phase front must become curved. When the taper length is long enough, the curved phase-front effect is negligible and the constant V-number concept is sufficient for designing a tapered waveguide. As the taper length decreases, the curved phase-front effect becomes important and should be taken into account. The influence of curved phase-front effect on the performance of tapered waveguides is discussed in Section III-C.

Transmission characteristics of an ideal tapered waveguide may be analyzed by employing the beam propagation method. Before carrying out the numerical simulation, it should be emphasized that the tapered waveguide under consideration is a 3-D case. The conformal mapping is, however, valid only for the 2-D transformation. Fortunately, methods for analyzing optical waveguides, such as the finite difference method, the finite element method, and the beam propagation method, usually need spatial discretization. For a 3-D straight waveguide (Fig. 3), spatial discretization along the direction of waveguide depth would result in several discrete φ $(\zeta - \eta)$ planes as shown in Fig. 2(b). Every discrete φ plane can be transformed into the χ $(z\text{-}x)$ plane of Fig. 2(a) by using (3) and (6). These mapped χ planes can be used to construct a 3-D analyzed space, in which the 3-D equivalent tapered waveguide is included. For any discrete φ plane, its 2-D Jacobian determinant $J_0(\zeta, \eta)$ is the same as those of other planes. Therefore, multiplying every discrete 2-D refractive-index distribution $\tilde{n}(\zeta, \eta)$ in the φ plane by the Jacobian determinant $J_0(\zeta, \eta)$, the 3-D index values in an ideal waveguide are derived.

Owing to neglecting the curved phase-front effect in the paraxial approximation, the beam propagation method based on the Fresnel equation cannot accurately simulate lightwave propagation in so-called wide-angle tapered structures [17]. Since a straight waveguide is equivalent to a completely adiabatic tapered waveguide, the investigation of ideal tapered

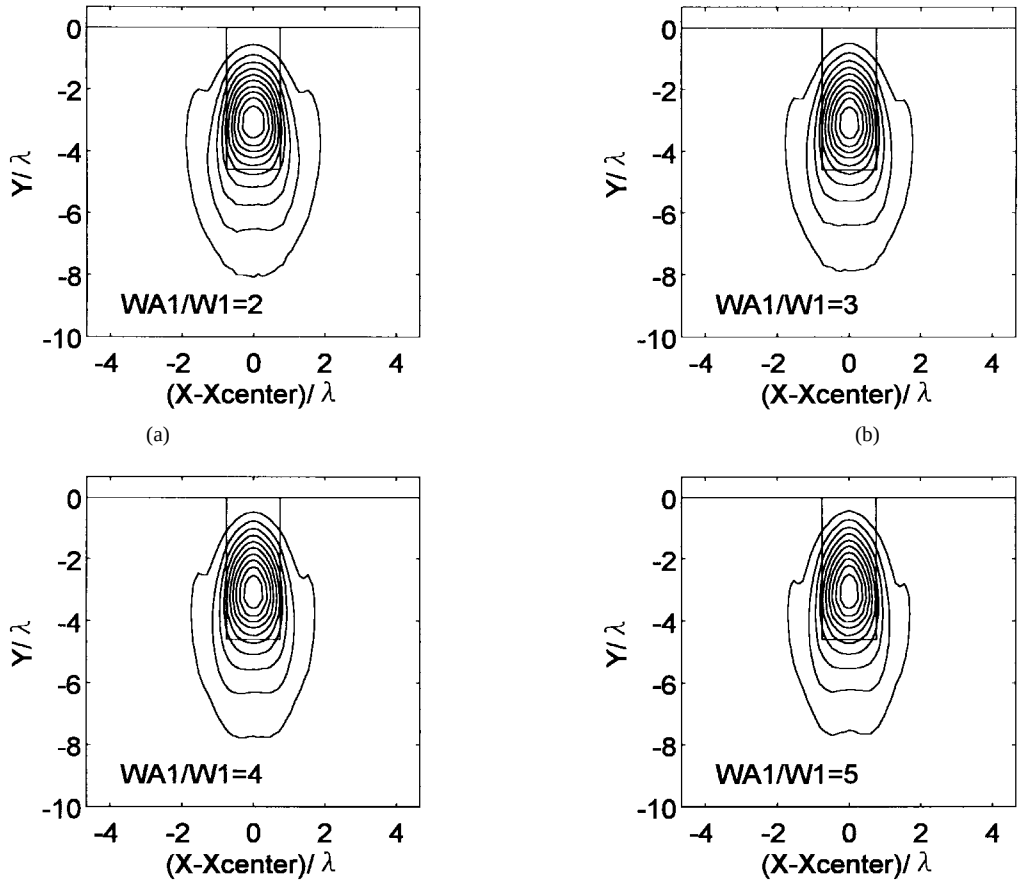

Fig. 12. The field intensity contours of the fundamental TE modes at the output ends of the constant V-number tapered waveguides with $W_1/W_2 = 4$ and (a) $W_{A1}/W_1 = 2$; (b) $W_{A1}/W_1 = 3$; (c) $W_{A1}/W_1 = 4$; (d) $W_{A1}/W_1 = 5$. Xcenter represents the lateral position of the center line.

waveguides can be substituted by analyzing corresponding straight structures. Notably, the analyzed domain shown in Fig. 2(a) represents a region where the refractive index should be altered to achieve a mode-size conversion. The analyzed domain may be not compatible with the computation window in simulations. When studying transmission characteristics of corresponding straight structures, the computation window should be correctly selected. The simulation results of the straight structure are then transformed into corresponding positions of the tapered waveguide. Thus, lightwave propagating in tapered structures is attained.

Fig. 9 indicates the wave propagation in an ideal tapered waveguide (the case of $W_1/W_2 = 4$ and $W_{A1} = 32\ \mu$m). The optical mode size gradually narrows as it crosses the tapered region. Moreover, the optical power at the output straight region condenses into a small area close to the center line. In addition, Fig. 10 depicts contour plots of transverse E-field intensity profiles at the input and output ends of the tapered waveguide (the case of $W_1/W_2 = 4$ and $W_{A1} = 32\ \mu$m). These two profiles clearly reveal that in this ideal structure a perfect mode-size conversion is achieved.

C. Influence of Curved Phase-Front Effect

To investigate the influence of curved phase-front effect on the performance of tapered waveguides explicitly, the optimal refractive-index distributions in completely adiabatic tapered waveguides (shown in Fig. 6) are replaced by different index distributions based on the constant V-number concept. Except the refractive-index distribution, the same waveguide shape and parameter values as those in ideal structures are chosen for numerical simulations. Fig. 11 shows the normalized field intensities (the solid lines with cross marked-points) at the output ends of constant V-number tapers with $W_1/W_2 = 4, W_{A1}/W_1 = 2, 3, 4$, and 5. In this figure, the solid lines with circle marked-points, used for comparing with the constant V-number cases, represent the normalized field intensities at the output ends of the corresponding ideal tapers. As can be seen in Fig. 6, the taper lengths of ideal structures with $W_1/W_2 = 4, W_{A1}/W_1 = 2, 3, 4$, and 5 are about 7.5, 10.5, 13.5, and 16.5 μm, respectively. When the taper length increases, the normalized transmitted power is gradually increased from 75.2 to 79.5%. This fact suggests that the curved phase-front effect is minished as the taper length increases. In Fig. 12, the variation in contour plots of transverse E-field intensity profiles at the output ends of constant V-number tapered waveguides (the cases of $W_1/W_2 = 4, W_{A1}/W_1 = 2, 3, 4$, and 5) are demonstrated. As illustrated in this figure, a better mode-size conversion is attained in a longer taper. Moreover, these contours are more broad as compared with the perfect intensity contour of Fig. 10(b). Therefore, the curved phase-front effect is an important factor in designing tapered waveguides.

IV. Conclusion

In this paper, a novel equivalent-waveguide concept that transforms a straight waveguide into an equivalent tapered structure has been proposed and applied to the design and analysis of completely adiabatic tapered waveguides. The equivalent structure offers the best insight into the mechanism of lightwave propagation in ideal tapered waveguides. Here, for the first time the curved phase-front effect in the taper is proposed to modify the constant V-number principle for designing tapered waveguides. The beam propagation method combined with the conformal mapping method is used to analyze the transmission characteristics of ideal structures. This improved algorithm avoids the errors caused by neglecting the curved phase-front effect when applying the paraxial approximation. Therefore, simulation results are useful for analyzing and designing the tapered waveguide structures in integrated optics.

References

[1] D. Marcuse, "Radiation losses of step-tapered channel waveguides," *Appl. Opt.*, vol. 19, pp. 3676–3681, Nov. 1980.

[2] R. N. Thurston, E. Kapon, and A. Shahar, "Two-dimensional control of mode size in optical channel waveguides by lateral channel tapering," *Opt. Lett.*, vol. 16, pp. 306–308, Mar. 1991.

[3] D. J. Vezzetti and M. Munowitz, "Design of strip-loaded optical waveguides for low-loss coupling to optical fibers," *J. Lightwave Technol.*, vol. 10, pp. 581–586, May 1992.

[4] H. Yanagawa, T. Shimizu, S. Nakamura, and I. Ohyama, "Index-and-dimensional taper and its application to photonic devices," *J. Lightwave Technol.*, vol. 10, pp. 587–591, May 1992.

[5] E. A. J. Marcatili, "Dielectric tapers with curved axes and no loss," *IEEE J. Quantum Electron.*, vol. 21, pp. 307–314, Apr. 1985.

[6] J. I. Sakai and E. A. J. Marcatili, "Lossless dielectric tapers with three-dimensional geometry," *J. Lightwave Technol.*, vol. 9, pp. 386–393, Mar. 1991.

[7] R. Weder, "Dielectric three-dimensional electromagnetic tapers with no loss," *IEEE J. Quantum Electron.*, vol. 24, pp. 775–779, May 1988.

[8] B. Chen, G. L. Tangonan, and A. Lee, "Horn structures for integrated optics," *Opt. Commun.*, vol. 20, pp. 250–252, Feb. 1977.

[9] W. K. Burns, A. F. Milton, and A. B. Lee, "Optical waveguide parabolic coupling horns," *Appl. Phys. Lett.*, vol. 30, pp. 28–30, Jan. 1977.

[10] O. Mitomi, K. Kasaya, and H. Miyazawa, "Design of a single-mode tapered waveguide for low-loss chip-to-fiber coupling," *IEEE J. Quantum Electron.*, vol. 30, pp. 1787–1793, Aug. 1994.

[11] P. G. Suchoski, Jr., and R. V. Ramaswamy, "Constant-width variable-index transition for efficient Ti-$LiNbO_3$ waveguide-fiber coupling," *J. Lightwave Technol.*, vol. 5, pp. 1246–1251, Sept. 1987.

[12] A. A. Lipovskii, "A taper coupler for integrated optics formed by ion-exchange under a nonuniform electric field," *Opt. Commun.*, vol. 61, pp. 11–15, Jan. 1987.

[13] N. Yamaguchi, Y. Kokubun, and K. Sato, "Low-loss spot-size transformer by dual tapered waveguides (DTW-SST)," *J. Lightwave Technol.*, vol. 8, pp. 587–593, Apr. 1990.

[14] S. J. Chung and C. H. Chen, "A partial variational approach for arbitrary discontinuities in planar dielectric waveguides," *IEEE Trans. Microwave Theory Tech.*, vol. 37, pp. 208–214, Jan. 1989.

[15] A. Weisshaar and V. K. Tripathi, "Modal analysis of step discontinuities in graded-index dielectric slab waveguides," *J. Lightwave Technol.*, vol. 10, pp. 593–602, May 1992.

[16] R. Baets and P. E. Lagasse, "Calculation of radiation loss in integrated-optic tapers and Y-junctions," *Appl. Opt.*, vol. 21, pp. 1972–1978, Jun. 1982.

[17] J. Yamauchi, Y. Akimoto, and M. Nibe, and H. Nakano, "Wide-angle propagating beam analysis for circularly symmetric waveguides: comparison between FD-BPM and FD-TDM," *IEEE Photon. Technol. Lett.*, vol. 8, pp. 236–238, Feb. 1996.

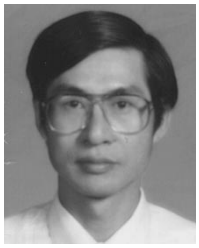

Ching-Ting Lee (M'89) was born in Taoyuan, Taiwan, Republic of China, on November 1, 1949. He received the B.S. and M.S. degrees in electrical engineering from the National Cheng-Kung University in 1972 and 1974, respectively. He received the Ph.D. degree in electrical engineering from Carnegie-Mellon University, Pittsburgh, PA, in 1982.

He worked in the Chung Shan Institute of Science and Technology and since 1990, he has been with the Institute of Optical Sciences, National Central University, Chung-Li, Taiwan, as a Professor. His current research interests include electro-optic integrated circuits and optics.

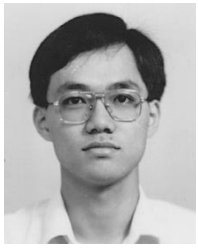

Mount-Learn Wu was born in Kaohsiung, Taiwan, Republic of China, on July 21, 1967. He received the B.S.E.E. degree from Feng-Chia University, Taichung, Taiwan, in 1990. He is currently working towards the Ph.D. degree in optical sciences at the Institute of Optical Sciences of National Central University, Chung-Li, Taiwan.

In September 1990, he joined the Institute of Optical Sciences of National Central University, Chung-Li, Taiwan, as a graduate student. His main interest is in integrated optical guided-wave devices.

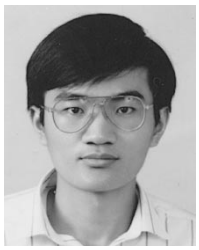

Lih-Gen Sheu was born in Taoyuan, Taiwan, Republic of China, on September 10, 1968. He received the B.S. degree in physics from the National Central University, Chung-Li, Taiwan, in 1990. He is currently working toward the Ph.D. degree at National Central University.

His research interests include the rare-earth-doped waveguide amplifiers and lasers.

Ping-Lin Fan was born in Taipei, Taiwan, Republic of China, on December 29, 1961. He received the B.S. degree in electrical engineering and the M.S. degree in optical science from the National Central University, Chung-Li, Taiwan, in 1985 and 1987, respectively. He is currently working toward the Ph.D. degree at National Central University.

His research interests include the design and applications of integrated-optic devices.

Jui-Ming Hsu was born in Nan-Toa, Taiwan, Republic of China, on February 14, 1955. He received the B.S.E.E. degree from Chung-Yuan University, Chung-Li, Taiwan, in 1978 and the M.S. degree from the Institute of Optical Science, National Central University, Chung-Li, Taiwan, in 1994. He is currently working toward the Ph.D. degree at National Central University.

His research interests include the design and applications of integrated-optic devices.